

Deep inelastic prompt photon production at HERA in the k_T -factorization approach

S.P. Baranov^a, A.V. Lipatov^b, N.P. Zotov^b

November 21, 2018

^a *P.N. Lebedev Physics Institute,
119991 Moscow, Russia*

^b *D.V. Skobeltsyn Institute of Nuclear Physics,
M.V. Lomonosov Moscow State University,
119991 Moscow, Russia*

Abstract

We investigate the prompt photon production in deep inelastic scattering at HERA in the framework of k_T -factorization QCD approach. Our study is based on the off-shell partonic amplitude $eq^* \rightarrow e\gamma q$, where the photon radiation from the leptons as well as from the quarks is taken into account. The unintegrated quark densities in a proton are determined using the Kimber-Martin-Ryskin prescription. The conservative error analysis is performed. We investigate both inclusive and jet associated prompt photon production rates. Our predictions are compared with the recent experimental data taken by the H1 and ZEUS collaborations. We demonstrate that in the k_T -factorization approach the contribution from the quark radiation subprocess (QQ mechanism) is enhanced as compared to the leading-order collinear approximation.

PACS number(s): 12.38.-t, 13.85.-t

1 Introduction

The production of prompt photons¹ in deep inelastic ep collisions at HERA is a subject of intense studies [1–3]. Such processes provide a direct probe of the hard subprocess dynamics, since the produced photons are largely insensitive to the effects of final-state hadronization.

¹Usually the photons are called "prompt" if they originate from hard interaction, not from the decay of final-state hadrons.

Studying the photon production in deep inelastic scattering (DIS) provides a test of perturbative Quantum Chromodynamics (QCD) with two hard scales: the transverse energy of the emitted photon E_T^γ , and the exchanged photon virtuality Q^2 . Good understanding of the production dynamics is also important for searches of new particles decaying to photons at the LHC conditions.

At the leading-order, the production of prompt photons in deep inelastic ep scattering is described by the parton-level process $eq \rightarrow e\gamma q$, where q represents a quark or an anti-quark, and e represents the beam lepton. The corresponding cross section $\sigma(ep \rightarrow e\gamma X)$ can be obtained by convoluting the parton-level cross section $\hat{\sigma}(eq \rightarrow e\gamma q)$ with the quark distribution functions in the proton. The observed final-state photon can be emitted by a quark or by a lepton (the so-called QQ and LL mechanisms, respectively). The interference contribution (LQ) is small. The QQ mechanism includes the direct photon radiation from the quark line and also the so-called fragmentation processes [4], where the produced quark forms a jet containing a photon with large fraction of the jet energy. This contribution involves poorly known quark-to-photon fragmentation functions $f_{q \rightarrow \gamma}(z)$ [5]. However, the isolation criterion introduced in experimental analyses² substantially reduces the fragmentation component [1–3].

Recently the H1 and ZEUS collaborations have reported their data [1–3] on the deep inelastic production of prompt photons at HERA, both inclusive and in association with a hadronic jet. The presented data on the inclusive prompt photon production have been compared [2, 3] with the LO pQCD $\mathcal{O}(\alpha^3)$ calculations [6]. A substantial (by a factor of about 2) disagreement between the data and theory has been found [3] at low Q^2 . Also, the absolute size of the reported experimental cross sections turned out to exceed the predictions of Monte-Carlo generators HERWIG [7] and PYTHIA [8] (by the factors of 7.9 and 2.3, respectively). Even after normalizing the total production rate, none of these programs was able to describe all kinematical dependences of the measured cross sections [1–3]. Comparison between the LO pQCD calculations [6] and the data in bins of η^γ shows that the difference can be attributed [3] mainly to the underestimation of the QQ contribution. At present, the next-to-leading order (NLO) $\mathcal{O}(\alpha^3\alpha_s)$ predictions are only available [9] for the associated photon plus jet phase space selection, yet not for inclusive process. These predictions are higher than the results of LO calculations [6], especially at low Q^2 , but still underestimate the data [3]. It was concluded [1–3] that further theoretical investigations (including the evaluation of higher-order processes) are needed to understand the observed discrepancy.

In the present paper to analyse the H1 and ZEUS data [1–3] we use instead the standard (collinear) approximation the so-called k_T -factorization [10] approach, which is based on Balitsky-Fadin-Kuraev-Lipatov (BFKL) [11] or Ciafaloni-Catani-Fiorani-Marchesini (CCFM) [12] evolution equations. A detailed description of the k_T -factorization approach can be found, for example, in the reviews [13]. Recently we have applied this approach to the inclusive and jet associated prompt photon photoproduction at HERA [14] and hadroproduction at Tevatron [15]. As it was demonstrated in the ZEUS paper [17] and also in the recent study [17] performed by the H1 collaboration, the k_T -factorization predictions are in better agreement with the data than collinear NLO calculations.

In the present study we extend our investigations [14] to the DIS region. We calculate

²See also Section 2.4.

the relevant off-shell (i.e. k_T -dependent) amplitude $\mathcal{M}(eq^* \rightarrow e\gamma q)$, where the virtuality of the incoming quarks is properly taken into account. Our consideration covers both the LL and QQ production mechanisms. We neglect the LQ mechanism since it gives only about 3% contribution to the total cross section. Then, we use the obtained expressions to calculate the total and differential cross sections of the deep inelastic production of prompt photons (both inclusive and accompanied by a hadronic jet). The unintegrated quark densities in a proton $f_q(x, \mathbf{k}_T^2, \mu^2)$ are taken in the Kimber-Martin-Ryskin (KMR) form [18]. We make a systematic comparison of our predictions to the available H1 and ZEUS data [1–3]. Our main goal is to study the capability of the k_T -factorization approach in describing the DIS data. Such calculations are performed for the first time.

The outline of our paper is the following. In Section 2 we recall shortly the basic formulas of the k_T -factorization approach with a brief review of the calculation steps. In Section 3 we present the numerical results of our calculations and a discussion. Section 4 contains our conclusions. The compact analytic expressions for the off-shell matrix elements of the $eq^* \rightarrow e\gamma q$ subprocess are given in the Appendix.

2 Theoretical framework

2.1 Off-shell amplitude of the $eq^* \rightarrow e\gamma q$ subprocess

Let us denote the four-momenta of the incoming electron and proton and the outgoing electron, photon and final quark by $p_e, p_p, p_{e'}, p_\gamma$ and p_q , respectively. The initial quark and virtual photon have four-momenta k and q .

Let us start with the LL production mechanism. There are two simple Feynman diagrams which describe this partonic subprocess at the leading order in α_{em} . The relevant matrix element reads

$$\mathcal{M}_{LL}(eq^* \rightarrow e\gamma q) = e_q e^3 \epsilon^\mu \frac{1}{q^2} L_{\mu\nu} H^\nu, \quad (1)$$

where e_q is the fractional electric charge of the quark and ϵ^μ is the produced photon polarization four-vector. The leptonic and hadronic tensors are given by the following expressions:

$$L^{\mu\nu} = \bar{u}(p_{e'}) \left[\gamma^\mu \frac{\hat{p}_{e'} + \hat{p}_\gamma + m_e}{(p_{e'} + p_\gamma)^2 - m_e^2} \gamma^\nu + \gamma^\nu \frac{\hat{p}_e - \hat{p}^\gamma + m_e}{(p_e - p^\gamma)^2 - m_e^2} \gamma^\mu \right] u(p_e), \quad (2)$$

$$H^\nu = \bar{u}(p_q) \gamma^\nu u(k). \quad (3)$$

When we calculate the matrix element squared, the summation over the produced photon polarizations is carried with $\sum \epsilon^\mu \epsilon^\nu = -g^{\mu\nu}$, and the spin density matrix for all on-shell spinors is taken in the standard form $u(p)\bar{u}(p) = \hat{p} + m$. In the case of off-shell initial quarks the on-shell spin density matrix has to be replaced with a more complicated expression. To evaluate it, we "extend" the original diagram and consider the off-shell quark line as internal line in the extended diagram. The "extended" process looks like follows: the initial on-shell quark with four-momentum p and mass m_q radiates a quantum (say, photon or gluon) and becomes an off-shell quark with four-momentum k . So, for the extended diagram squared we write:

$$|\mathcal{M}|^2 \sim \text{Sp} \left[\bar{\mathcal{T}}^\mu \frac{\hat{k} + m_q}{k^2 - m_q^2} \gamma^\nu u(p)\bar{u}(p) \gamma_\nu \frac{\hat{k} + m_q}{k^2 - m_q^2} \mathcal{T}_\mu \right], \quad (4)$$

where \mathcal{T} is the rest of the original matrix element which remains unchanged. The expression presented between $\bar{\mathcal{T}}^\mu$ and \mathcal{T}_μ now plays the role of the off-shell quark spin density matrix. Using the on-shell condition $u(p)\bar{u}(p) = \hat{p} + m_q$ and performing the Dirac algebra one obtains in the massless limit $m_q \rightarrow 0$:

$$|\mathcal{M}|^2 \sim \frac{1}{(k^2)^2} \bar{\mathcal{T}}^\mu \left(2k^2 \hat{p} - 4(p \cdot k) \hat{k} \right) \mathcal{T}_\mu. \quad (5)$$

Now we use the Sudakov decomposition $k = xp + k_T$ and neglect the second term in the parentheses in (5) in the small- x limit to arrive at

$$|\mathcal{M}|^2 \sim \frac{2}{xk^2} \bar{\mathcal{T}}^\mu x \hat{p} \mathcal{T}_\mu. \quad (6)$$

(Essentially, we have neglected here the negative light-cone momentum fraction of the incoming quark). The properly normalized off-shell spin density matrix is given by $x\hat{p}$, while the factor $2/xk^2$ has to be attributed to the quark distribution function (determining its leading behavior). With this normalization, we successfully recover the on-shell collinear limit when k is collinear with p .

The evaluation of traces was done using the algebraic manipulation system FORM [19]. The expression for $|\bar{\mathcal{M}}_{QQ}(eq^* \rightarrow e\gamma q)|^2$ can be easily obtained from (1) — (3) if we replace $p_e \rightarrow k$, $p_{e'} \rightarrow p_q$, $k \rightarrow p_e$, $p_q \rightarrow p_{e'}$ and multiply (1) by an extra factor e_q . For the reader's convenience, we collect the analytic formulas for the off-shell matrix elements $|\bar{\mathcal{M}}_{LL}(eq^* \rightarrow e\gamma q)|^2$ and $|\bar{\mathcal{M}}_{QQ}(eq^* \rightarrow e\gamma q)|^2$ in the Appendix.

2.2 Cross section for the prompt photon production

According to the k_T -factorization theorem, the cross section of the process $ep \rightarrow e\gamma X$ can be written as a convolution of the off-shell matrix element $|\bar{\mathcal{M}}(eq^* \rightarrow e\gamma q)|^2$ and unintegrated quark distribution $f_q(x, \mathbf{k}_T^2, \mu^2)$:

$$\begin{aligned} \sigma_{LL,QQ}(ep \rightarrow e\gamma X) &= \sum_q \int \frac{1}{256\pi^3 x^2 s \sqrt{s} |\mathbf{p}_{\gamma T}| \exp(y_\gamma)} |\bar{\mathcal{M}}_{LL,QQ}(eq^* \rightarrow e\gamma q)|^2 \times \\ &\times f_q(x, \mathbf{k}_T^2, \mu^2) d\mathbf{p}_{e'T}^2 d\mathbf{p}_{qT}^2 d\mathbf{k}_T^2 dy_{e'} dy_q \frac{d\phi_{e'}}{2\pi} \frac{d\phi_q}{2\pi} \frac{d\phi}{2\pi}, \end{aligned} \quad (7)$$

where $y_{e'}$, y_q and $\phi_{e'}$ and ϕ_q are the center-of-mass rapidities and azimuthal angles of the outgoing electron and (anti)quark, respectively. The rapidity y_γ of the produced photon is given by

$$y_\gamma = \ln \left[\frac{\sqrt{s} - m_{e'T} \exp(y_{e'}) - m_{qT} \exp(y_q)}{|\mathbf{p}_{\gamma T}|} \right], \quad (8)$$

where $m_{e'T}$ and m_{qT} are the transverse masses of the corresponding particles. We note that averaging the expression (7) over ϕ and taking the limit $\mathbf{k}_T^2 \rightarrow 0$ we recover the well-known LO result of collinear parton model. We use the unintegrated quark densities in a proton $f_q(x, \mathbf{k}_T^2, \mu^2)$ taken in the KMR form [18]. The KMR approach is a formalism to construct the unintegrated parton (quark and gluon) distributions from the known conventional parton

distributions $xa(x, \mu^2)$, where $a = g$ or $a = q$. For the input, we have used the recent leading-order Martin-Stirling-Thorne-Watt (MSTW) [20] parton densities.

As it is often done for deep inelastic prompt photon production, we choose the renormalization and factorization scales to be $\mu^2 = \xi Q^2$. In order to estimate the theoretical uncertainties of our calculations we vary the scale parameter ξ between 1/2 and 2 about the default value $\xi = 1$. We use the LO formula for the strong coupling constant $\alpha_s(\mu^2)$ with $n_f = 4$ active (massless) quark flavours and $\Lambda_{\text{QCD}} = 200$ MeV, such that $\alpha_s(M_Z^2) = 0.1232$.

The multidimensional integration in (7) has been performed by the means of Monte Carlo technique, using the routine VEGAS [21]. The full C++ code is available from the authors on request³.

2.3 Fragmentation contributions

Perturbation theory becomes nonapplicable when the wavelength of the emitted photon (in the emitting quark rest frame) becomes larger than the typical hadronic scale \mathcal{O} (1 GeV⁻¹). Then the nonperturbative effects of hadronization or fragmentation must be taken into account. Accordingly, the calculated cross section can be split into two pieces

$$d\sigma = d\sigma_{\text{direct}}(\mu^2) + d\sigma_{\text{fragm}}(\mu^2) \quad (9)$$

with $d\sigma_{\text{direct}}(\mu^2)$ representing the perturbative contribution and $d\sigma_{\text{fragm}}(\mu^2)$ the fragmentation contribution. In our calculations we choose the fragmentation scale μ^2 to be the invariant mass of the quark + photon subsystem, $\mu^2 = (p + p_i)^2$, and restrict $d\sigma_{\text{direct}}(\mu^2)$ to $\mu \geq M \simeq 1$ GeV. Under this condition, the contribution $d\sigma_{\text{direct}}(\mu^2)$ is free from divergences. We have checked that the sensitivity of our results to the choice of M is reasonably soft. As far as the fragmentation contribution is concerned, its size is dramatically reduced by the photon isolation cuts (see below). According to the estimates presented in [22], the contribution from $d\sigma_{\text{fragm}}$ amounts to only few percent of the visible cross section. This value is smaller than the theoretical uncertainty in the perturbative contribution $d\sigma_{\text{direct}}$, and so, is neglected in our analysis.

2.4 Photon isolation cuts

In order to reduce huge background from the secondary photons produced by the decays of π^0 and η mesons the isolation criterion is introduced in the experimental analyses. This criterion is the following. A photon is isolated if the amount of hadronic transverse energy E_T^{had} , deposited inside a cone with aperture R centered around the photon direction in the pseudo-rapidity and azimuthal angle plane, is smaller than some value E_T^{max} :

$$\begin{aligned} \sum_{\text{had}} E_T^{\text{had}} &\leq E_T^{\text{max}}, \\ (\eta^{\text{had}} - \eta)^2 + (\phi^{\text{had}} - \phi)^2 &\leq R^2. \end{aligned} \quad (10)$$

Both the H1 and ZEUS collaborations take $R \sim 1.0$ and $E_T^{\text{max}} \sim 1$ GeV [1–3]. Isolation not only reduces the background from light hadron decays but also significantly reduces the

³lipatov@theory.sinp.msu.ru

fragmentation components connected with collinear photon radiation. It was shown that after applying the isolation cut (10) the contribution from the fragmentation subprocesses is suppressed [22].

3 Numerical results

3.1 Inclusive production

Experimental data on the deep inelastic inclusive prompt photon production come from both the ZEUS and H1 collaborations. The differential cross sections are measured as function of the produced photon transverse energy E_T^γ , pseudo-rapidity η^γ , exchanged photon virtuality Q^2 and Bjorken variable x . The ZEUS data [1] refer to the kinematic region defined as $5 < E_T^\gamma < 10$ GeV, $-0.7 < \eta^\gamma < 0.9$, $Q^2 > 35$ GeV², $E_e' > 10$ GeV, $139.8^\circ < \theta_e' < 171.8^\circ$. The initial electron and proton energies are $E_e = 27.6$ GeV and $E_p = 920$ GeV. The E_e' and θ_e' are the energy and the polar angle of the scattered electron⁴. Another, very recent set [2] of the ZEUS data, refers to the kinematic region $4 < E_T^\gamma < 15$ GeV, $-0.7 < \eta^\gamma < 0.9$, $10 < Q^2 < 350$ GeV², $E_e' > 10$ GeV, $139.8^\circ < \theta_e' < 171.9^\circ$. The invariant mass of the final state hadronic system $W_X > 5$ GeV. The H1 data [3] refer to the kinematic region $3 < E_T^\gamma < 10$ GeV, $-1.2 < \eta^\gamma < 1.8$, $4 < Q^2 < 150$ GeV², $E_e' > 10$ GeV, $153 < \theta_e' < 177$, $y > 0.05$. Additionally, the H1 data on the transverse energy distributions have been divided into five subdivisions of η^γ , namely $-1.2 < \eta^\gamma < -0.6$, $-0.6 < \eta^\gamma < 0.2$, $0.2 < \eta^\gamma < 0.9$, $0.9 < \eta^\gamma < 1.4$ and $1.4 < \eta^\gamma < 1.8$. To suppress the contribution from the elastic Compton scattering a cut on the mass of the final state hadronic system $W_X > 50$ GeV is applied.

Our predictions on the differential cross sections as a function of transverse energy E_T^γ , pseudo-rapidity η^γ , Q^2 and x variables are shown in Figs. 1 — 5 in comparison with the data [1–3]. Solid histograms are obtained by fixing both the factorization and normalization scales at the default value $\mu^2 = Q^2$, whereas the upper and lower dashed histograms correspond to the scale variation as it was described above. We find that the predicted cross sections agree well with the H1 and ZEUS data both in the normalization and shape. A slight underestimation of the H1 data is only observed at high Q^2 . In general, the k_T -factorization predictions describe the data much better than the LO collinear calculations.

Our calculations give for the total cross sections $47.7_{-1.5}^{+1.3}$ pb, $6.1_{-0.3}^{+0.3}$ pb and $22.0_{-0.9}^{+0.7}$ pb for the H1 [3], ZEUS [1] and ZEUS [2] kinematic regions, respectively. The experimentally measured cross sections are 50.3 ± 1.7 (stat.) $_{-7.8}^{+6.8}$ (syst.) pb, 5.64 ± 0.58 (stat.) $_{-0.72}^{+0.47}$ (syst.) pb and 19.4 ± 0.7 (stat.) $_{-1.0}^{+1.2}$ (syst.) pb. The collinear LO pQCD predictions are 28.6 pb and 5.39 pb for the H1 [3] and ZEUS [1] kinematical regions. Besides that, the sole QQ contribution has been extracted in the ZEUS experiment [2] giving 12.2 ± 0.7 (stat.) $_{-1.0}^{+1.2}$ (syst.) pb. Our prediction of $14.8_{-0.5}^{+0.4}$ pb is very close to this value. We find that the QQ contribution yields about 65% of the total cross section. In the collinear LO calculations this mechanism gives only about 50%. The reason for the enhancement of the QQ contribution in the k_T -factorization approach can be seen in the fact that the unintegrated parton (quark) distribution effectively include a large piece of higher-order corrections. According to the

⁴All kinematic variables are given in the laboratory frame where the positive direction of the OZ axis is given by the proton beam.

observation of [3], the difference between the collinear LO calculations and the data can mainly be attributed to an underestimation of the QQ contribution.

The dependence of our results on the renormalization/factorization scale μ^2 on its own weak, leading to about 5% uncertainty band over a wide kinematic range. We cannot estimate the uncertainty connected with the choice of unintegrated quark distributions (although, it may be potentially much larger) because, at the time being, they are only available in the KMR scheme⁵ (see also reviews [13] for more information).

3.2 Production in association with a jet

To calculate the jet-associated production of prompt photons we apply the procedure used previously in [24]. The produced photon is accompanied by a number of partons radiated in the course of the parton evolution. On the average, the parton transverse momentum decreases from the hard interaction block towards the proton. As an approximation, we assume that the parton with momentum k' emitted at the last evolution step compensates the transverse momentum of the parton participating in the hard subprocess, i.e. $\mathbf{k}'_T \simeq -\mathbf{k}_T$. All the other emitted partons are collected together in the proton remnant, which is assumed to carry only a negligible transverse momentum compared to \mathbf{k}'_T . This parton gives rise to a final hadron jet with $E_T^{\text{jet}} = |\mathbf{k}'_T|$, in addition to the jet produced in the hard subprocess. From these hadron jets we choose the one carrying the largest transverse energy.

Experimental data for this process have been obtained by the H1 and ZEUS collaborations. The ZEUS collaboration presented the cross sections [1] measured in the kinematic region $5 < E_T^\gamma < 10$ GeV, $E_T^{\text{jet}} > 6$ GeV, $-0.7 < \eta^\gamma < 0.9$, $-1.5 < \eta^{\text{jet}} < 1.8$, $Q^2 > 35$ GeV², $E'_e > 10$ GeV, $139.8^\circ < \theta'_e < 171.8^\circ$ with electron energy $E_e = 27.6$ GeV and proton energy $E_p = 920$ GeV. The more recent H1 data [3] refer to the kinematic region $3 < E_T^\gamma < 10$ GeV, $E_T^{\text{jet}} > 2.5$ GeV, $-1.2 < \eta^\gamma < 1.8$, $-1.0 < \eta^{\text{jet}} < 2.1$, $4 < Q^2 < 150$ GeV², $E'_e > 10$ GeV, $153^\circ < \theta'_e < 177^\circ$, $y > 0.05$ and $W_X > 50$ GeV with the same electron and proton energies.

The results of our calculations are shown in Figs. 6 and 7 in comparison with the HERA data. One can see that the distributions measured by the H1 collaboration are well reproduced by our calculations. However, our results overshoot the earlier ZEUS data. A possible reason for that can be connected with the jet selection algorithm, being the consequence of the used approximations. Another possible reason is that our calculations are restricted to the parton level only, while the jet fragmentation mechanism could also be of importance. Concerning the collinear NLO predictions, the shapes of the differential cross sections $d\sigma/dE_T^\gamma$, $d\sigma/d\eta^\gamma$ and $d\sigma/dQ^2$ are described well, but the normalization is too low, by about 40% [3]. The difference between the LO and NLO predictions is mostly concentrated at low Q^2 [3].

The calculated total cross sections $\sigma(ep \rightarrow e\gamma + \text{jet}) = 33.2^{+0.9}_{-1.0}$ pb and $1.9^{+0.1}_{-0.1}$ pb have to be compared with 31.6 ± 1.2 (stat.) $^{+4.2}_{-4.8}$ (syst.) pb and 0.86 ± 0.14 (stat.) $^{+0.44}_{-0.34}$ (syst.) pb, measured by the H1 and ZEUS collaborations in the relevant kinematic regions. We find perfect agreement between our predictions and recent H1 data. A sizeable overestimation of the ZEUS data is observed. It seems that the consistency of the H1 and ZEUS data with each other can be questioned. The total cross sections calculated in the collinear approximation at the LO and NLO level for H1 conditions are 16.7 pb and 20.2 pb, respectively [3].

⁵Several attempts to calculate the CCFM-evolved unintegrated quark densities were made in [23].

As the final point, we should mention that corrections for hadronisation and multiple interactions have been taken into account in the NLO analysis of the HERA data [1–3] performed in the framework of collinear factorization. The correction factors are typically 0.8 — 1.2 depending on a bin. These corrections are not taken into account in our consideration.

4 Conclusions

We have investigated the deep inelastic production of prompt photons at HERA in the k_T -factorization approach. Our study is based on the off-shell partonic amplitude $eq^* \rightarrow e\gamma q$, where the photon radiation from the leptons as well as from the quarks is taken into account. The unintegrated quark densities in a proton are calculated using the Kimber-Martin-Ryskin prescription.

We have studied both the inclusive and jet associated production of prompt photons. Our numerical predictions on the inclusive production cross sections are in well agreement with the H1 and ZEUS data. We have demonstrated that in the k_T -factorization approach the role of the QQ contribution is enhanced compared to the collinear LO approximation of QCD. Our results for the jet associated production agree with the H1 measurements but overshoot the ZEUS data. Probably, there exists a problem of incompatibility of these H1 and ZEUS data with each other.

Acknowledgements

The authors are very grateful to DESY Directorate for the support in the framework of Moscow — DESY project on Monte-Carlo implementation for HERA — LHC. A.V.L. was supported in part by the grants of the president of Russian Federation (MK-432.2008.2) and Helmholtz — Russia Joint Research Group. Also this research was supported by the FASI of Russian Federation (grant NS-1456.2008.2), FASI state contract 02.740.11.0244 and RFBR grant 08-02-00896-a.

5 Appendix

Here we present compact analytic expressions for the matrix elements involved in (7). In the massless limit, the squared off-shell matrix elements $|\bar{\mathcal{M}}_{LL,QQ}(eq^* \rightarrow e\gamma q)|^2$ summed over the final states and averaged over the initial states are

$$|\bar{\mathcal{M}}_{LL}|^2 = \frac{(4\pi\alpha_{em})^3 e_q^2 x}{16(k^2 - 2(p_q \cdot k))^2} \left[\frac{F_{LL}^{(1)}}{(p^\gamma \cdot p_{e'})^2} + \frac{F_{LL}^{(2)}}{(p^\gamma \cdot p_e)^2} + \frac{2F_{LL}^{(12)}}{(p^\gamma \cdot p_e)(p^\gamma \cdot p_{e'})} \right], \quad (A.1)$$

$$|\bar{\mathcal{M}}_{QQ}|^2 = \frac{(4\pi\alpha_{em})^3 e_q^4 x}{64(p_e \cdot p_{e'})^2} \left[\frac{F_{QQ}^{(1)}}{(p^\gamma \cdot p_q)^2} + \frac{F_{QQ}^{(2)}}{((p^\gamma \cdot k) - k^2)^2} + \frac{2F_{QQ}^{(12)}}{(p^\gamma \cdot p_q)((p^\gamma \cdot k) - k^2)} \right], \quad (A.2)$$

where

$$F_{LL}^{(1)} = 128(p^\gamma \cdot p_q)(p^\gamma \cdot p_{e'})(p_e \cdot p_p) + 128(p^\gamma \cdot p_{e'})(p^\gamma \cdot p_p)(p_q \cdot p_e), \quad (A.3)$$

$$F_{LL}^{(2)} = 128(p^\gamma \cdot p_q)(p^\gamma \cdot p_e)(p_e \cdot p_p) + 128(p^\gamma \cdot p_e)(p^\gamma \cdot p_p)(p_q \cdot p_{e'}), \quad (A.4)$$

$$\begin{aligned} F_{LL}^{(12)} = & -64(p^\gamma \cdot p_q)(p_e \cdot p_{e'})(p_e \cdot p_p) + 64(p^\gamma \cdot p_q)(p_e \cdot p_{e'})(p_e \cdot p_p) - \\ & 64(p^\gamma \cdot p_e)(p_q \cdot p_e)(p_e \cdot p_p) - 64(p^\gamma \cdot p_e)(p_q \cdot p_{e'})(p_e \cdot p_p) - \\ & 128(p^\gamma \cdot p_e)(p_q \cdot p_{e'})(p_e \cdot p_p) + 128(p^\gamma \cdot p_{e'})(p_q \cdot p_e)(p_e \cdot p_p) + \\ & 64(p^\gamma \cdot p_{e'})(p_q \cdot p_e)(p_e \cdot p_p) + 64(p^\gamma \cdot p_{e'})(p_q \cdot p_{e'})(p_e \cdot p_p) - \\ & 64(p^\gamma \cdot p_p)(p_q \cdot p_e)(p_e \cdot p_{e'}) + 64(p^\gamma \cdot p_p)(p_q \cdot p_{e'})(p_e \cdot p_{e'}) - \\ & 128(p_q \cdot p_e)(p_e \cdot p_{e'})(p_e \cdot p_p) - 128(p_q \cdot p_{e'})(p_e \cdot p_{e'})(p_e \cdot p_p), \end{aligned} \quad (A.5)$$

$$F_{QQ}^{(1)} = 128(p^\gamma \cdot p_q)(p^\gamma \cdot p_e)(p_{e'} \cdot p_p) + 128(p^\gamma \cdot p_q)(p^\gamma \cdot p_{e'})(p_e \cdot p_p), \quad (A.6)$$

$$\begin{aligned} F_{QQ}^{(2)} = & 128(p^\gamma \cdot p_e)(p^\gamma \cdot p_p)(p_q \cdot p_{e'}) + 128(p^\gamma \cdot p_{e'})(p^\gamma \cdot p_p)(p_q \cdot p_e) + \\ & 128(p^\gamma \cdot k)(p_q \cdot p_e)(p_{e'} \cdot p_p) + 128(p^\gamma \cdot k)(p_q \cdot p_{e'})(p_e \cdot p_p) - \\ & 128(p^\gamma \cdot p_p)(p_q \cdot p_e)(p_{e'} \cdot k) - 128(p^\gamma \cdot p_p)(p_q \cdot p_{e'})(p_e \cdot k) - \\ & 64(p_q \cdot p_e)(p_{e'} \cdot p_p)k^2 - 64(p_q \cdot p_{e'})(p_e \cdot p_p)k^2, \end{aligned} \quad (A.7)$$

$$\begin{aligned} F_{QQ}^{(12)} = & 64(p^\gamma \cdot p_q)(p_q \cdot p_e)(p_{e'} \cdot p_p) + 64(p^\gamma \cdot p_q)(p_q \cdot p_{e'})(p_e \cdot p_p) + \\ & 64(p^\gamma \cdot p_q)(p_e \cdot k)(p_{e'} \cdot p_p) + 64(p^\gamma \cdot p_q)(p_e \cdot p_p)(p_{e'} \cdot k) + \\ & 64(p^\gamma \cdot p_e)(p_q \cdot p_{e'})(p_q \cdot p_p) - 64(p^\gamma \cdot p_e)(p_q \cdot k)(p_{e'} \cdot p_p) + \\ & 64(p^\gamma \cdot p_{e'})(p_q \cdot p_e)(p_q \cdot p_p) - 64(p^\gamma \cdot p_{e'})(p_q \cdot k)(p_e \cdot p_p) - \\ & 64(p^\gamma \cdot k)(p_q \cdot p_p)(p_e \cdot p_{e'}) - 128(p^\gamma \cdot p_p)(p_q \cdot p_e)(p_q \cdot p_{e'}) - \\ & 64(p^\gamma \cdot p_p)(p_q \cdot p_e)(p_{e'} \cdot k) - 64(p^\gamma \cdot p_p)(p_q \cdot p_{e'})(p_e \cdot k) + \\ & 64(p^\gamma \cdot p_p)(p_q \cdot k)(p_e \cdot p_{e'}) - 64(p_q \cdot p_e)(p_q \cdot k)(p_{e'} \cdot p_p) - \\ & 64(p_q \cdot p_e)(p_q \cdot p_p)(p_{e'} \cdot k) - 64(p_q \cdot p_{e'})(p_q \cdot k)(p_e \cdot p_p) - \\ & 64(p_q \cdot p_{e'})(p_q \cdot p_p)(p_e \cdot k). \end{aligned} \quad (A.8)$$

References

- [1] S. Chekanov *et al.* (ZEUS Collaboration), Phys. Lett. B **595**, 86 (2004).
- [2] S. Chekanov *et al.* (ZEUS Collaboration), arXiv:0909.4223 [hep-ex].
- [3] F.D. Aaron *et al.* (H1 Collaboration), Eur. Phys. J. C **54**, 371 (2008).
- [4] K. Koller, T.F. Walsh, and P.M. Zerwas, Z. Phys. C **2**, 197 (1979).
- [5] A. Gehrmann-De Ridder, G. Kramer, and H. Spiesberger, Eur. Phys. J. C **11**, 137 (1999).
- [6] A. Gehrmann-De Ridder, T. Gehrmann, and E. Poulsen, Phys. Rev. Lett. **96**, 132006 (2006).
- [7] G. Marchesini *et al.*, Comp. Phys. Comm. **67**, 465 (1992).
- [8] T. Sjostrand *et al.*, Comp. Phys. Comm. **135**, 238 (2001).
- [9] A. Gehrmann-De Ridder, G. Kramer, and H. Spiesberger, Nucl. Phys. B **578**, 326 (2000).
- [10] L.V. Gribov, E.M. Levin, and M.G. Ryskin, Phys. Rep. **100**, 1 (1983);
E.M. Levin, M.G. Ryskin, Yu.M. Shabelsky and A.G. Shuvaev, Sov. J. Nucl. Phys. **53**, 657 (1991);
S. Catani, M. Ciafaloni and F. Hautmann, Nucl. Phys. B **366**, 135 (1991);
J.C. Collins and R.K. Ellis, Nucl. Phys. B **360**, 3 (1991).
- [11] E.A. Kuraev, L.N. Lipatov and V.S. Fadin, Sov. Phys. JETP **44**, 443 (1976);
E.A. Kuraev, L.N. Lipatov and V.S. Fadin, Sov. Phys. JETP **45**, 199 (1977);
I.I. Balitsky and L.N. Lipatov, Sov. J. Nucl. Phys. **28**, 822 (1978).
- [12] M. Ciafaloni, Nucl. Phys. B **296**, 49 (1988);
S. Catani, F. Fiorani and G. Marchesini, Phys. Lett. B **234**, 339 (1990);
S. Catani, F. Fiorani and G. Marchesini, Nucl. Phys. B **336**, 18 (1990);
G. Marchesini, Nucl. Phys. B **445**, 49 (1995).
- [13] B. Andersson *et al.* (Small- x Collaboration), Eur. Phys. J. C **25**, 77 (2002);
J. Andersen *et al.* (Small- x Collaboration), Eur. Phys. J. C **35**, 67 (2004);
J. Andersen *et al.* (Small- x Collaboration), Eur. Phys. J. C **48**, 53 (2006).
- [14] A.V. Lipatov and N.P. Zotov, Phys. Rev. D **72**, 054002 (2005).
- [15] A.V. Lipatov and N.P. Zotov, J. Phys. G **34**, 219 (2007);
S.P. Baranov, A.V. Lipatov, and N.P. Zotov, Phys. Rev. D **77**, 074024 (2008);
S.P. Baranov, A.V. Lipatov, and N.P. Zotov, Eur. Phys. J. C **56**, 371 (2008).
- [16] S. Chekanov *et al.* (ZEUS Collaboration), Eur. Phys. J. C **49**, 511 (2007).
- [17] F.D. Aaron *et al.* (H1 Collaboration), arXiv:0910.5631 [hep-ex].

- [18] M.A. Kimber, A.D. Martin, and M.G. Ryskin, Phys. Rev. D **63**, 114027 (2001);
G. Watt, A.D. Martin, and M.G. Ryskin, Eur. Phys. J. C **31**, 73 (2003).
- [19] J.A.M. Vermaseren, "Symbolic Manipulation with FORM", published by Computer Algebra Nederland, Kruislaan 413, 1098, SJ Amsterdam, 1991; ISBN 90-74116-01-9.
- [20] A.D. Martin, W.J. Stirling, R.S. Thorne, and G. Watt, arXiv:0901.0002 [hep-ph].
- [21] G.P. Lepage, J. Comput. Phys. **27**, 192 (1978).
- [22] H. Baer, J. Ohnemus, and J.F. Owens, Phys. Rev. D **42**, 61 (1990);
P. Aurenche, M. Fontannaz, J.Ph. Guillet, E. Pilon, and M. Werlen, Phys. Rev. D **73**,
094007 (2006).
- [23] A.V. Lipatov and N.P. Zotov, arXiv:0907.3303 [hep-ph].
- [24] S.P. Baranov and N.P. Zotov, Phys. Lett. B **491**, 111 (2000).

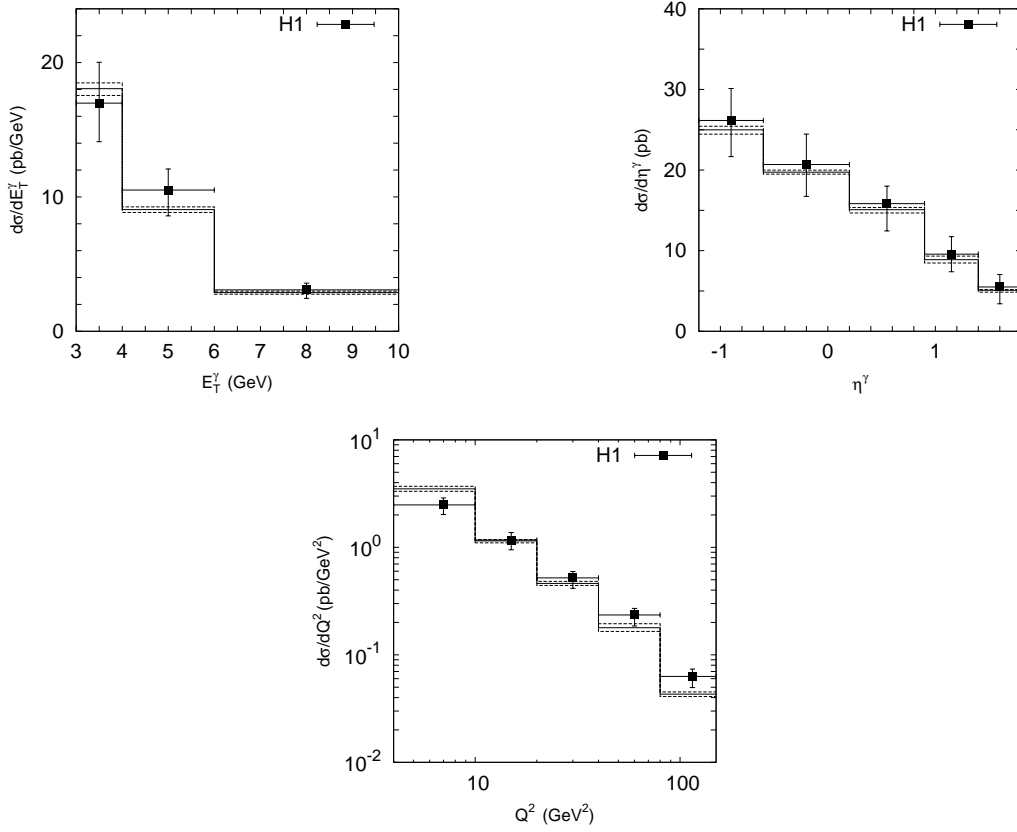


Figure 1: Differential cross sections of the inclusive deep inelastic prompt photon production as a function of E_T^γ , η^γ and Q^2 calculated at $3 < E_T^\gamma < 10$ GeV, $-1.2 < \eta^\gamma < 1.8$, $4 < Q^2 < 150$ GeV², $E_e' > 10$ GeV, $153^\circ < \theta_e' < 177^\circ$, $y > 0.05$ and $W_X > 50$ GeV. The solid histogram corresponds to the default scale $\mu^2 = Q^2$, whereas the upper and lower dashed histograms correspond to scale variations described in the text. The experimental data are from H1 [3].

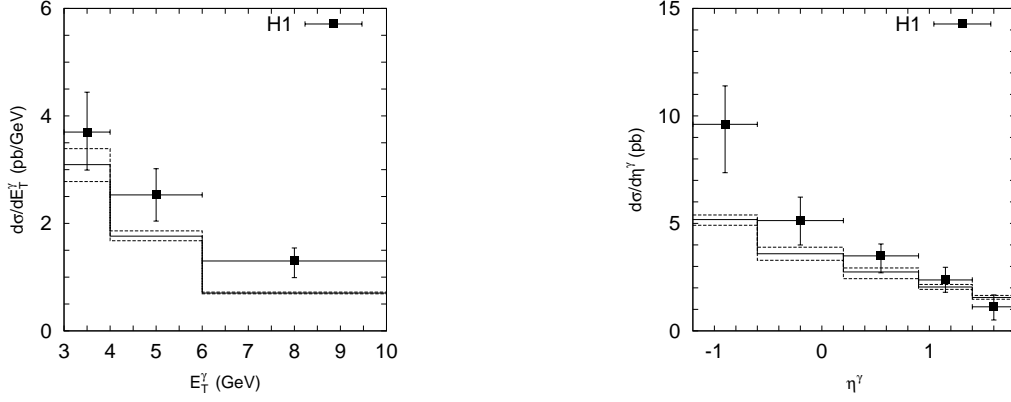


Figure 2: Differential cross sections of the deep inelastic inclusive prompt photon production as a function of E_T^γ and η^γ calculated at $3 < E_T^\gamma < 10$ GeV, $-1.2 < \eta^\gamma < 1.8$, $40 < Q^2 < 150$ GeV², $E_e' > 10$ GeV, $153^\circ < \theta_e' < 177^\circ$, $y > 0.05$ and $W_X > 50$ GeV. Notation of the histograms is as in Fig. 1. The experimental data are from H1 [3].

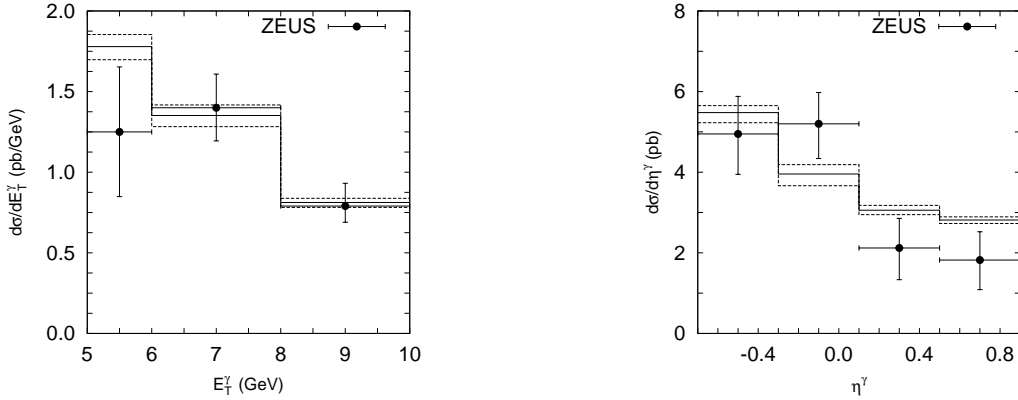


Figure 3: Differential cross sections of the deep inelastic inclusive prompt photon production as a function of E_T^γ and η^γ calculated at $5 < E_T^\gamma < 10$ GeV, $-0.7 < \eta^\gamma < 0.9$, $Q^2 > 35$ GeV², $E_e' > 10$ GeV and $139.8^\circ < \theta_e' < 171.8^\circ$. Notation of the histograms is as in Fig. 1. The experimental data are from ZEUS [1].

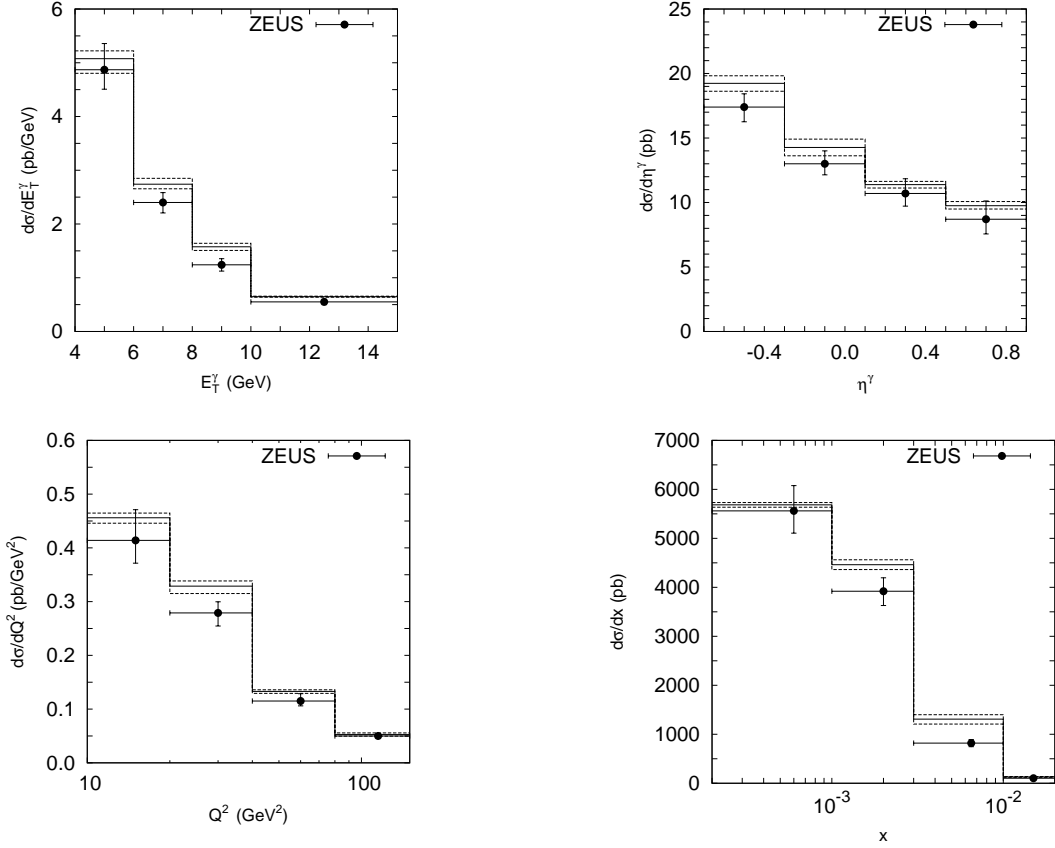


Figure 4: Differential cross sections of the inclusive deep inelastic prompt photon production at HERA as a function of E_T^γ , η^γ , Q^2 and x calculated at $4 < E_T^\gamma < 15$ GeV, $-0.7 < \eta^\gamma < 0.9$, $10 < Q^2 < 350$ GeV², $E_e' > 10$ GeV, $139.8^\circ < \theta_e' < 171.9^\circ$ and $W_X > 5$ GeV. Notation of the histograms is as in Fig. 1. The experimental data are from ZEUS [2].

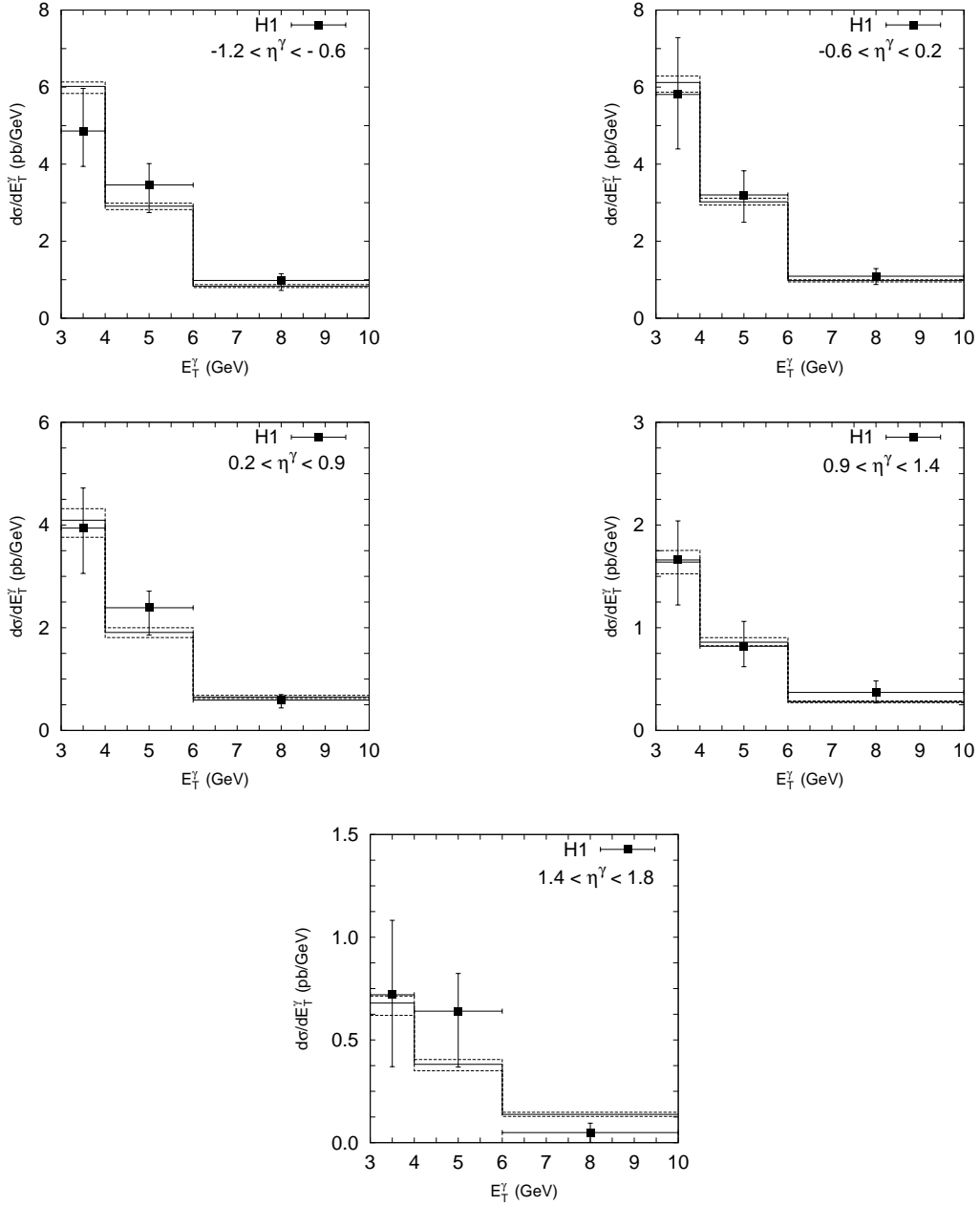


Figure 5: Differential cross sections of the deep inelastic inclusive prompt photon production as a function of E_T^γ calculated for different subdivisions of the η^γ range. Notation of the histograms is as in Fig. 1. The experimental data are from H1 [3].

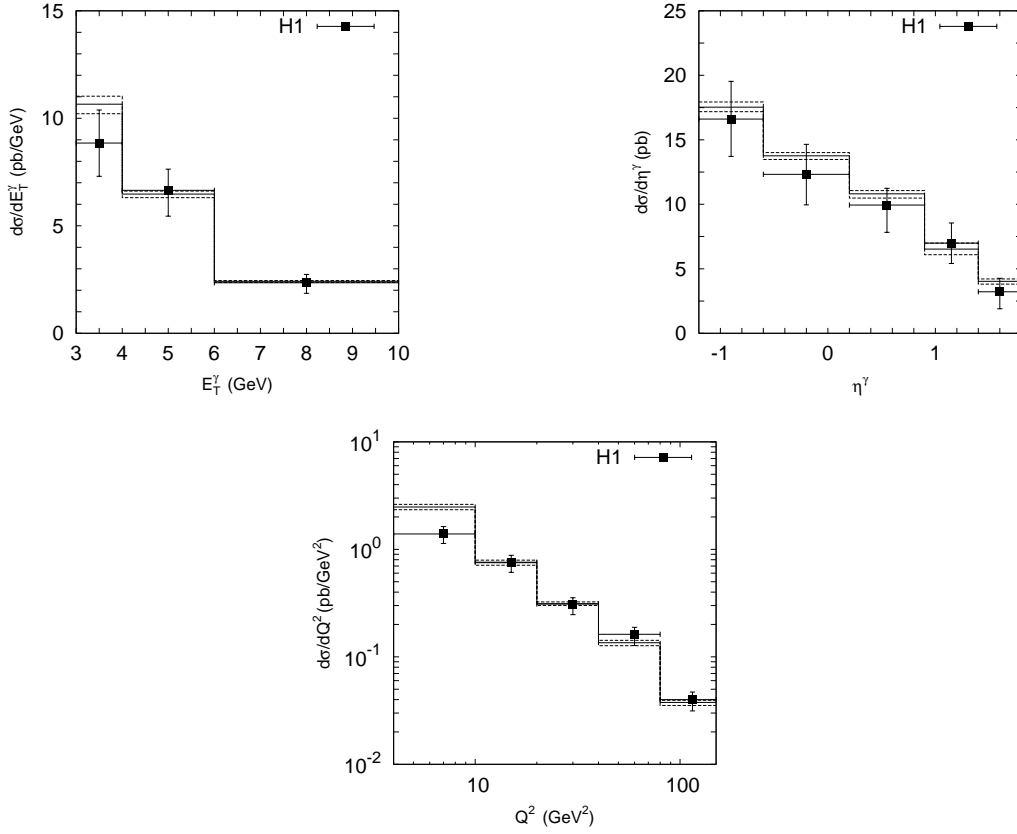


Figure 6: Differential cross sections of the deep inelastic prompt photon and jet associated production as a function of E_T^γ , η^γ and Q^2 calculated at $3 < E_T^\gamma < 10$ GeV, $E_T^{\text{jet}} > 2.5$ GeV, $-1.2 < \eta^\gamma < 1.8$, $-1.0 < \eta^{\text{jet}} < 2.1$, $4 < Q^2 < 150$ GeV², $E_e' > 10$ GeV, $153^\circ < \theta_e' < 177^\circ$, $y > 0.05$ and $W_X > 50$ GeV. Notation of the histograms is as in Fig. 1. The experimental data are from H1 [3].

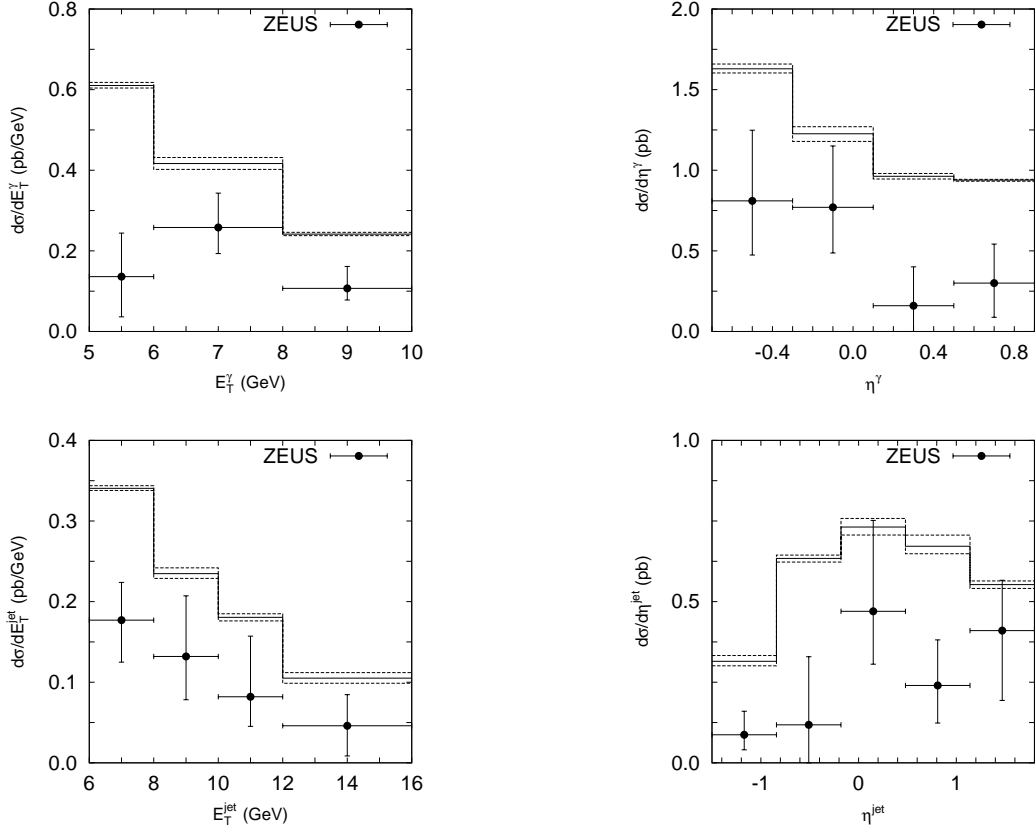


Figure 7: Differential cross sections of the deep inelastic prompt photon and jet associated production as a function of E_T^γ , η^γ , E_T^{jet} and η^{jet} calculated at $5 < E_T^\gamma < 10$ GeV, $E_T^{\text{jet}} > 6$ GeV, $-0.7 < \eta^\gamma < 0.9$, $-1.5 < \eta^{\text{jet}} < 1.8$, $Q^2 > 35$ GeV², $E'_e > 10$ GeV and $139.8^\circ < \theta'_e < 171.8^\circ$. Notation of the histograms is as in Fig. 1. The experimental data are from ZEUS [1].